



An experimental study of the role of shear deformation on partial melting of a synthetic metapelite

Elizaveta Tumarkina^{a,*}, Santanu Misra^a, Luigi Burlini^a, James A.D. Connolly^b

^a Structural Geology and Tectonics group, Geological Institute, ETH, Sonneggstrasse 5, Zurich 8092, Switzerland

^b Institute of Geochemistry and Petrology, ETH, Clausiusstrasse 25, Zurich 8092, Switzerland

ARTICLE INFO

Article history:

Received 31 March 2010

Received in revised form 6 December 2010

Accepted 14 December 2010

Available online 22 December 2010

Keywords:

Reaction kinetics

Partial melting

Rock deformation

Shear heating

Effective viscosity

Torsion experiment

ABSTRACT

Experiments on a synthetic, foliated, quartz-muscovite rock were undertaken to evaluate and explain the influence of shear deformation on partial melting at 750 °C and 300 MPa. Torsion experiments were conducted at a constant strain rate of $3 \times 10^{-4} \text{ s}^{-1}$ with the initial foliation parallel and orthogonal to the direction of applied angular displacement. The non-equilibrium melting reaction forms melt, sillimanite, biotite, and K-feldspar at the expense of muscovite and quartz. In both static and torsion experiments, for the first 1.5 h the rate of melting is identical, thereafter melting accelerates in the torsion experiments. The rate of melting is highest in torsion experiments with the sample foliation orthogonal to the shear plane. First order models for shear heating, surface and strain energy, and mean stress effects suggest that none of these effects explain the difference in melting rate between static and torsion experiments. We conclude that the most probable explanation for the correlation between reaction rate and shear deformation is that shear deformation lowers the effective viscosity of the rock matrix. The reduction in effective viscosity facilitates the elimination of the grain-scale mean-stress perturbations caused by the volume change of the melting reaction. As these perturbations inhibit reaction, their elimination by ductile dilational deformation accelerates the melting process.

© 2010 Elsevier B.V. All rights reserved.

1. Introduction

Metapelitic rocks have a strong influence on the mechanical behaviour of continental crust. A number of studies have been undertaken to understand metamorphic reactions in metapelites. These studies include hydrostatic experimental investigations (Kerrick, 1972; Huang and Wyllie, 1974; Vielzeuf and Holloway, 1988; Rubie and Brearley, 1987; Haselton et al., 1995), theoretical calculations (Grant, 1973; Thompson and Algor, 1977; Thompson, 1982; Clemens and Vielzeuf, 1987) and field-based studies (Barbey et al., 1990; Berger and Kalt, 1999). In the domain of metamorphism of pelites, partial melting is one of the fundamental processes by which the crust differentiates and provides important geological information on crustal evolution (Davidson et al., 1994; Rutter, 1997; Rushmer, 2001). The melting of muscovite-, biotite- and hornblende-bearing rocks under fluid-absent conditions involves the break-down of hydrous minerals to produce partial melt and a less hydrous restite (e.g., granulites, Johannes and Holtz, 1996). Hydrous minerals have long been recognized as the source of water-bearing granitic magmas (Huang and Wyllie, 1973; Grant,

1973; Clemens, 1984 etc). Thompson (1982) reported the replacement of iron-rich muscovite by either biotite, cordierite or garnet during fluid-absent melting depending on pressure conditions. Rubie and Brearley (1987) and Brearley and Rubie (1990) investigated metastable melting during the breakdown of muscovite + quartz from partial melting to crystallization of new phases at 680°–757 °C under both fluid-present and fluid-absent conditions. Under fluid-absent conditions, the muscovite + quartz breakdown reaction leads directly to K-feldspar + sillimanite + biotite + H₂O (melt). In the presence of water muscovite becomes completely replaced by melt + corundum + mullite + biotite, which subsequently reacts to melt + mullite + biotite. Most of the studies investigating dehydration melting of pelitic composition had either muscovite or biotite or both in the assemblages. According to Rushmer (2001) and Holyoke and Rushmer (2002) reactions of muscovite and biotite are different by reaction kinetics and volume change associated with dehydration melting. The melt generation is faster during muscovite dehydration. Experimental studies under hydrostatic conditions observe a large positive volume change associated with dehydration melting of muscovite (Connolly et al., 1997; Rushmer, 2001; Holyoke and Rushmer, 2002).

Most of the aforementioned investigations did not consider the role of deformation in detail. Rather, these studies characterized the role of pressure and temperature in crystallisation and melting. However,

* Corresponding author. Tel.: +41 44 632 88 23; fax: +41 44 632 10 80.
E-mail address: elizaveta.tumarkina@erdw.ethz.ch (E. Tumarkina).

regional metamorphism of pelites is generally associated with crustal deformation due to tectonic stress. Regions of melt production coincide with active tectonic belts, because melt production and segregation rates changes significantly in the presence of deformation (Rushmer, 2001; Misra et al., 2009). De Ronde and Stünitz (2007) showed that deformation enhances diffusion-controlled reaction of anorthite + forsterite = orthopyroxene + clinopyroxene + spinel. Keller et al. (2004) described reactions progress more rapidly in shear zones than in surrounding undeformed regions in a polymetamorphic metapelite (Monte Rosa nappe, Western Alps). They explained the difference in terms of kinetics by H₂O-saturated conditions in the shear zone compared to fluid-unsaturated in the host-rock, with high water activity enhanced diffusion of chemical elements. However, the question of behaviour of melt-composed muscovite systems during the deformation processes is not yet understood, despite the fact that muscovite is an important rock-forming mineral in a large variety of metamorphic rocks. Moreover, muscovite dehydration melting is an important source of granites during high grade metamorphism. To date there have been no detailed studies on the effect of large strain deformation on melt-bearing system. A Paterson-type gas-medium testing machine equipped with torsion actuator provides the means to undertake experiments to large shear strain. Therefore, in this work we have investigated the role of deformation in simple shear on a quartz-muscovite bearing system at constant confining pressure and temperature. Samples with different initial foliation orientation were deformed from low to high finite shear strains at constant displacement rate. Hydrostatic experiments were conducted with the same starting material, timing and pressure-temperature conditions to isolate the hydrostatic from non-hydrostatic microstructures and reaction kinetics.

2. Experimental methods

2.1. Starting material and sample preparation

Synthetic samples were fabricated from 30 vol.% of quartz and 70 vol.% of muscovite powders obtained from Alberto Luisoni (<http://www.a-luisoni.ch/>). The size of quartz grains was 6–12 μm and muscovite flakes were 30–34 μm in length (measured with a Master-Sizer 2000). The densities were 2.65 gm/cm³ and 2.82 gm/cm³ of quartz and muscovite, respectively (measured with a helium gas pycnometer, AccuPyc 1300). The chemical composition of quartz is very pure, SiO₂; muscovite is phengitic in character with composition (K_{0.9}Na_{0.1})(Al_{1.6}Fe_{0.3}Mg_{0.1})[Si_{3.2}Al_{0.8}O₁₀](OH)₂, measured in an electron microprobe.

Quartz and muscovite powders were mixed and pressed uniaxially at 200 MPa at room temperature inside a steel canister. During the uniaxial cold press, the flaky muscovite grains aligned orthogonal to the compression direction developing a planar fabric (foliation). Afterwards, the material underwent HIP (Hot Isostatic Pressing) at 165 MPa and 590 °C for 30 h and produced synthetic rock. During the uniaxial cold press, the flaky muscovite grains aligned orthogonal to the compression direction developing a planar fabric (foliation). X-ray diffraction (XRD), X-ray fluorescence (XRF) and electron microprobe analyses performed on the starting material indicated that the hot-pressed starting material used in all subsequent deformation and hydrostatic experiments contained only quartz and muscovite. Two types of cylindrical specimens with 10 mm in diameter and 3–5 mm in length were cored keeping the foliation either parallel or perpendicular with respect to the cylinder axis (Fig. 1a).

2.2. Deformation apparatus and sample assembly

All experiments were performed in an internally heated, Paterson type gas-medium testing machine, equipped with torsion actuator (Paterson and Olgaard, 2000). The specimen is placed between two 3 mm thick solid alumina spacers adjacent to alumina and zirconia

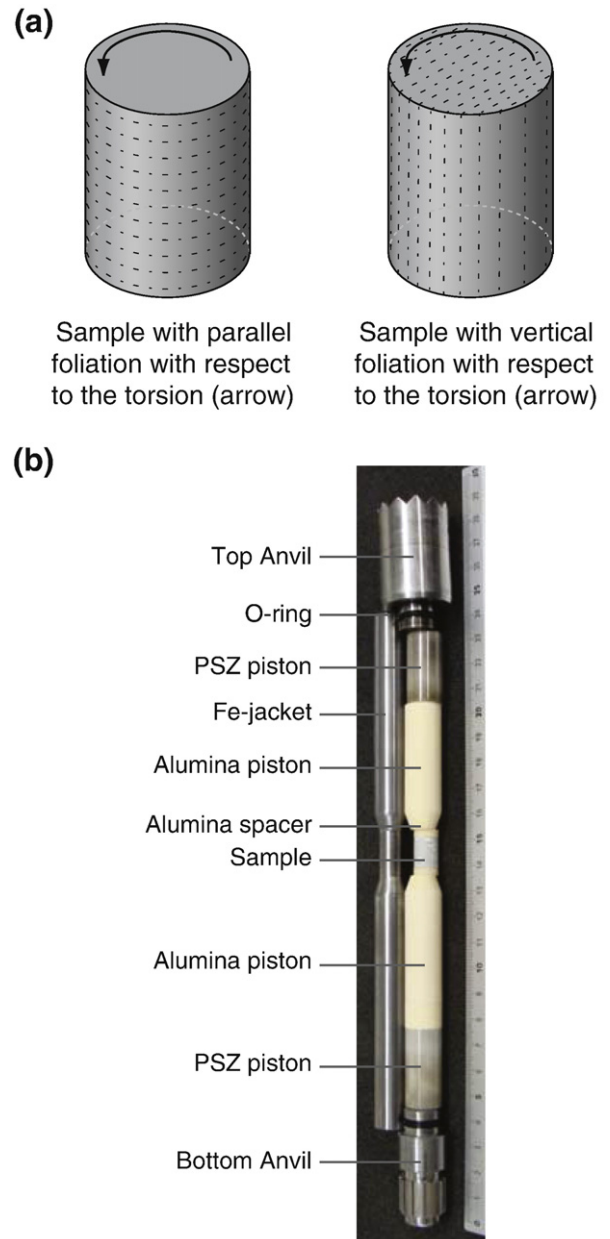


Fig. 1. (a) A schematic illustration of samples with different initial foliations. The orientation of the foliations is shown as dashed lines (not to scale); (b) photograph of typical sample assembly used in this study.

pistons with continuous 2 mm hole for the thermocouple in the middle (Fig. 1b). The solid spacers are used to limit the loss of fluids through the thermocouple hole. The zirconia and alumina pistons help to attain a stable thermal profile along the sample and reduce conductive heat loss away from the sample. The assembly is inserted into a Fe-jacket to isolate the sample and pistons from the confining medium. Temperature is measured with K-type thermocouples placed 3 mm from the top of the specimen. Straight grooves were scratched on the jacket along the axis of the whole assembly as passive strain markers.

2.3. Experimental conditions

Two types of experiments were performed; hydrostatic and torsion (dynamic). In hydrostatic experiments temperature and confining pressure were held constant at 750 °C and 300 MPa, respectively. In

torsion experiments, the samples were deformed under same confining pressure and temperature of a hydrostatic experiments with constant shear strain rate ($\dot{\gamma}$) of $3 \times 10^{-4} \text{ s}^{-1}$ applied over different durations to achieve various magnitudes of finite shear strain (γ). The time required to deform a sample to $\gamma=1$ at $3 \times 10^{-4} \text{ s}^{-1}$ was approximately 1 hour. Two types of torsion experiments were performed; the first type was with muscovite foliation parallel to the torsion direction, the second type was with normal to the torsion direction muscovite foliation (Fig. 1a). The duration of the experiments was 1 to 5 h for hydrostatic experiments and 1 to 7 h for the torsion tests.

2.4. Methods of analysis

Longitudinal sections, tangential to the outer edge of both the hydrostatic and deformed samples, were prepared for SEM and electron microprobe analyses. This location corresponds to the zone of maximum shear strain in deformed samples (Paterson and Olgaard, 2000). They were observed with both, SE (secondary electron) and BSE (backscattered electron) modes. The greyscale contrasts of the BSE images have been used to determine the area percentage of melt. Both manual (for low contrast images) and digital (for high contrast images) techniques were used to measure this percentage. In manual mode the areas of melt were marked on a transparency sheet over the selected BSE image; the marked areas were then digitized to a binary image. In digital mode, the BSE images were transferred directly to a binary image with a suitable tolerance value for selecting only the melt areas. Image analysis software (ImageJ) was used to quantify the area percentage of melt. In each sample 4 to 6 different areas around $400 \mu\text{m}^2$ in size were analysed. A comparative study between manual and digital processes found that the difference is negligible ($\pm 1.8\%$).

3. Results

The results of the hydrostatic and the torsion experiments are summarized in Table 1.

3.1. Hydrostatic experiments

Two types of phengitic muscovite were observed in the hydrostatic experiment held at conditions (750 °C/300 MPa) for one hour

Table 1
Summary of conducted experiments. All of the experiments have been conducted at 300 MPa and 750 °C. Abbreviations—Mus: muscovite; Qtz: quartz; L: melt; Sil: sillimanite; Bt: biotite; Kfs: potassium feldspar.

| N of experiment | Shear strain | Time (hours) | Mica initial orientation (in respect to the torsion direction) | Phases | Melt amount ($\pm 2\%$) |
|-----------------|--------------|--------------|--|------------------------|---------------------------|
| 1123 | Hydrostatic | 1 | – | Mus+Qtz | – |
| 1121 | Hydrostatic | 2 | – | Mus+Qtz+L+Sil+Bt | 7 |
| 1122 | Hydrostatic | 5 | – | Mus+Qtz+L+Sil+Bt+Kfs | 13 |
| 1013 | 1 | 0.93 | Parallel | Mus+Qtz | – |
| 1026 | 3 | 2.78 | Parallel | Mus+Qtz+L+Sil+Bt+Kfs | 11 |
| 1025 | 7 | 6.48 | Parallel | Qtz+L+Sil+Bt+Kfs(+Mus) | 22 |
| 1084 | 1 | 0.93 | Perpendicular | Mus+Qtz | – |
| 1085 | 1.5 | 1.39 | Perpendicular | Mus+Qtz(+L+Sil+Bt) | – |
| 1129 | 3 | 2.78 | Perpendicular | Mus+Qtz+L+Sil+Bt | 20 |
| 1082 | 5 | 4.63 | Perpendicular | Mus+Qtz+L+Sil+Bt+Kfs | 21 |

(P1123, Table 1). The muscovites are visible in BSE SEM-images (Fig. 2a). The brightest in BSE images are the Fe-rich type of phengite, which has around 6 mass % FeO, darker Fe-poor type has around 3 mass % FeO according to the electron microprobe analyses.

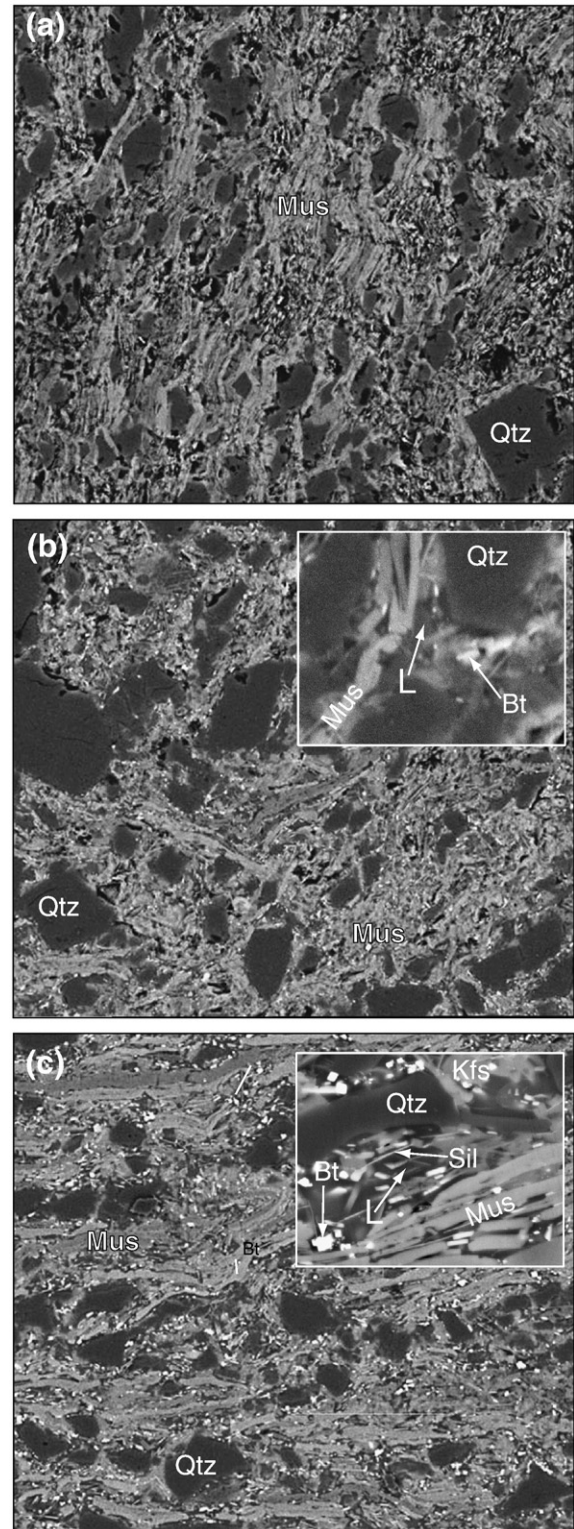


Fig. 2. Evolution of melting and crystallization processes with progressing time in hydrostatic experiments at 300 MPa and 750 °C. (a), (b) and (c) are experiments for 1, 2 and 5 h (width of the images: 60 μm). The inset images in (b) and (c) show new crystals and melt in high magnification (width of the images: 10 μm). Abbreviations—Mus: muscovite; Qtz: quartz; L: melt; Bt: biotite; Kfs: potassium feldspar; Sil: sillimanite.

After two hours (P1121) the original muscovite is replaced by an iron-rich and iron-poor phengitic muscovite. Small melt pockets (around 7 area %, diameter $\sim 1 \mu\text{m}$), are observed along grain boundaries (Fig. 2b, inset). Likewise, the melt is associated with small fibrous crystals with a length of $ca 1 \mu\text{m}$, which XRD analysis reveals to be sillimanite. A few new-formed elongate biotite grains, $ca 0.5 \mu\text{m}$ in size are also present in the system.

After 5 h (P1122) (Fig. 2) the amounts of melt, sillimanite and biotite are increasing in comparison with previous experiment. K-feldspar grains are also developing. Melt is present in both isolated pockets and as continuous melt films along the grain boundaries (amount of melt is $ca 13$ area %). In addition, sillimanite crystals reach $2 \mu\text{m}$ in length and biotite crystals are $ca 1 \mu\text{m}$ in size (Fig. 2c).

3.2. Torsion experiments

3.2.1. Samples with foliation parallel to the torsion direction

Experiments were performed at 750°C and 300 MPa to different finite shear strains. At $\gamma = 1$ (P1013) only three mineral phases are observed, quartz and two phengitic muscovites (Fig. 3a). The observations are the same as in the hydrostatic experiments with the same duration. Muscovite crystal sizes range from 10 to $20 \mu\text{m}$ in length and grains are gently bent and kinked.

With progressive shearing ($\gamma = 3$, P1026) muscovite breakdown is indicated by the appearance of a few melt pockets along grain boundaries (around 10% of whole area) (Fig. 3b). Melt pockets contain sillimanite crystals. Bright (on the BSE images) and very small, less than $0.5 \mu\text{m}$, elongate biotite crystals are also observed along the grain boundaries of muscovite and quartz. Additionally, a few K-feldspar grains, isometric and $ca 2 \mu\text{m}$ in diameter, are observed.

At higher shear strain ($\gamma = 7$) (P1025) most of the phengite crystals do not observed in the sample and melting is prominent (around 20–22 area %) (Fig. 3c). Melt pockets are interconnected, and form a continuous network. The composition of melt is very acidic, 70–80 wt.% SiO_2 , 15–20 wt.% Al_2O_3 and 2–5 wt.% K_2O . The melt areas contain sillimanite (up to $1 \mu\text{m}$ in length), K-feldspar (up to $5 \mu\text{m}$) and elongate biotite crystals up to $2 \mu\text{m}$ in length. The biotite crystals are enriched in Fe (~ 15 wt.% FeO) relative to the initial muscovite composition (~ 5 wt.% in FeO).

3.2.2. Samples with foliation normal to torsion direction

At $\gamma = 1$ (P1084) quartz and two types of phengitic muscovite are observed (Fig. 4a) as in the experiment (P1013) with foliation parallel to the shear plane at the corresponding shear strain. At $\gamma = 1.5$, (P1085) muscovite and quartz react to form melt pockets of about $1 \mu\text{m}$ in size (less than 5 area %). Small sillimanite crystals are observed inside these pockets. New biotite crystals were also observed along grain boundaries of muscovite and quartz. Biotite crystals are $< 0.5 \mu\text{m}$.

At increased shear strain ($\gamma = 3$, P1129) the melt content (20 area %) is significantly greater than at $\gamma = 1$. Moreover, melt starts to accumulate in elongate shear bands (Fig. 4b). At higher shear strain ($\gamma = 5$, P1082) melt pockets are significantly greater than in previous experiment (around 23 area %) and contain long sillimanite fibers (1 – $2 \mu\text{m}$), biotite (almost $1 \mu\text{m}$ in size) and K-feldspar crystals ($ca 2 \mu\text{m}$ in average diameter) (Fig. 4c).

The mechanical behaviour of the torsion experiments is summarized in a shear stress versus shear strain plot (Fig. 5a). Regardless of the initial orientation of the foliation, the deformation starts with elastic hardening, reaches the stress peak around shear strain $\gamma = 0.5$ – 1.0 , then melting causes weakening and in the case of foliation parallel to shear plane from shear strain equal to 2.5 – 3.0 mechanical equilibrium is achieved. In the experiments with foliation perpendicular to the direction of shearing samples continue to strain weaken, but at a lower rate, from gamma around 2 to the end of the experiment.

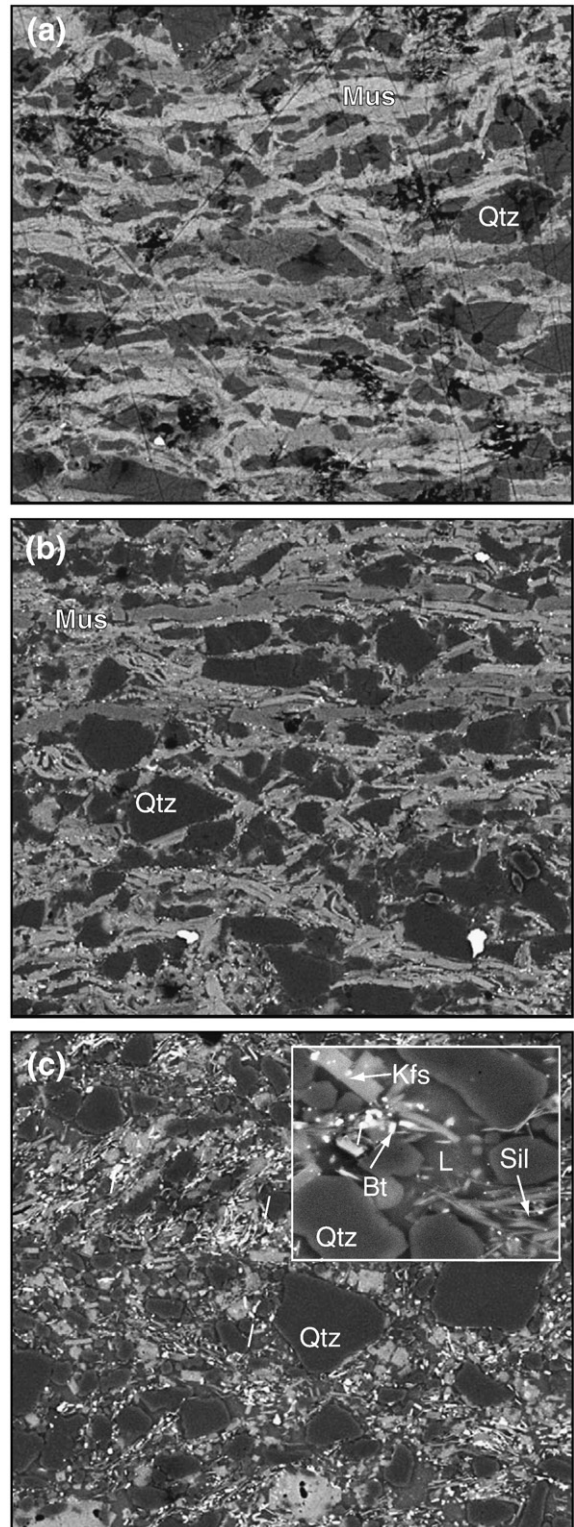


Fig. 3. Evolution of melting and crystallization processes with progressing shearing in torsion experiments of samples with foliation parallel to torsion direction at 300 MPa and 750°C . Longitudinal tangential surfaces of deformed cylindrical samples were cut, polished and observed under SEM with BSE mode. The magnitude of finite shear strain (γ) in (a), (b) and (c) are 1, 3 and 7, respectively (width of the images: $60 \mu\text{m}$). The inset image (width: $10 \mu\text{m}$) in (c) shows different phases including melt in higher magnification. In all images, the shear direction is top to the right. Abbreviations—Mus: muscovite; Qtz: quartz; L: melt; Bt: biotite; Kfs: potassium feldspar.

The area percentages of partial melt were measured for all the experiments, following the way as described before, and the data were plotted versus time (Fig. 6). The rate of melting is independent

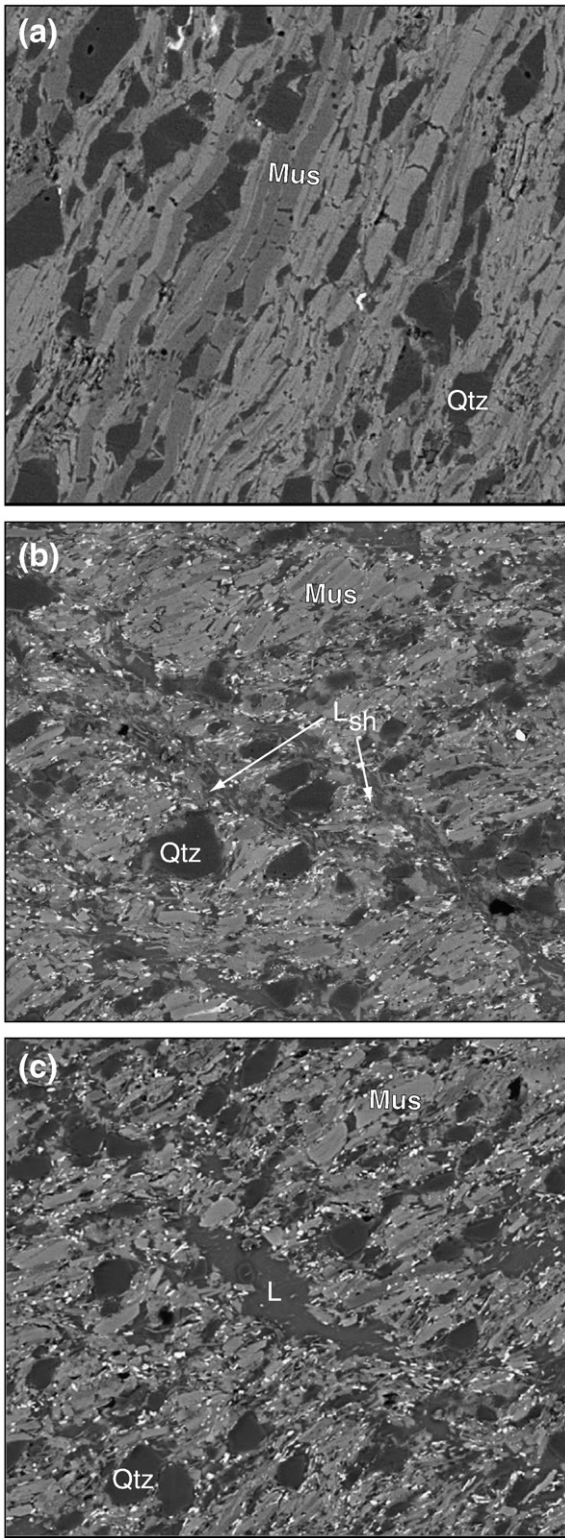


Fig. 4. Evolution of melting and crystallization processes during torsion experiments of samples with foliation perpendicular to torsion direction at 300 MPa and 750 °C. Longitudinal tangential surfaces of deformed cylindrical samples were cut, polished and observed under SEM with BSE mode. The magnitude of finite shear strain (γ) in (a), (b) and (c) are 1, 3 and 5, respectively (width of the images: 60 μm). In (b) and (c) crystals of biotite are visible by tiny white spots. In all images, the shear direction is top to the right. Abbreviations—Mus: muscovite; Qtz: quartz; L: melt; L_{sh} : melt rich shear band.

on the imposed conditions (hydrostatic/dynamic) during the first 1.5 h of experiments (Fig. 6). After this time, imposed conditions gradually influence rate of melting. The results also indicate that the initial muscovite foliation affects the reaction kinetics (Fig. 6).

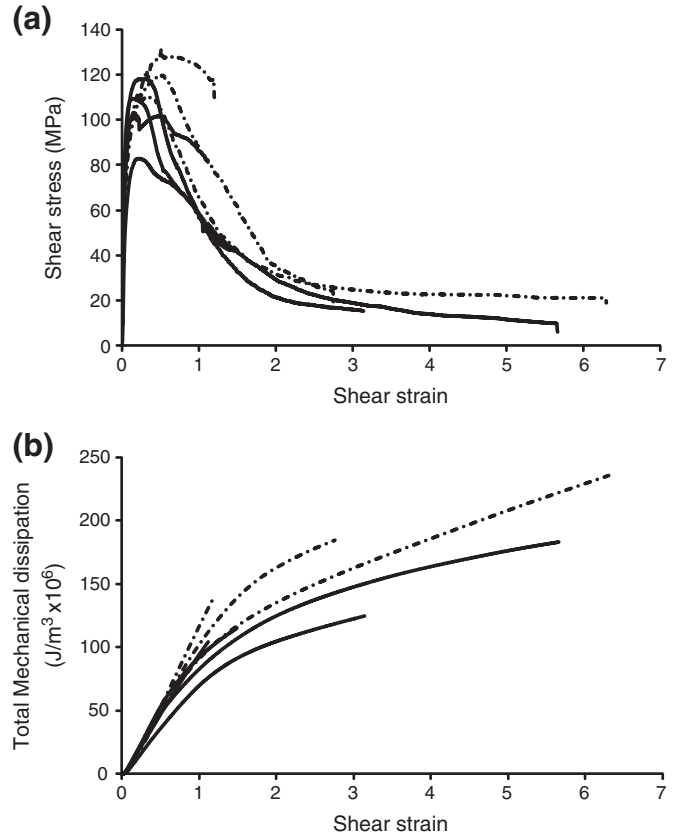


Fig. 5. (a) Mechanical data of torsion experiments, shear stress versus shear strain. Dashed curves represent torsion experiments with foliation parallel to the torsion direction; solid curves represent torsion experiments with foliation perpendicular to the torsion direction. (b) Plot of mechanical dissipation versus shear strain. Dashed curves represent torsion experiments with foliation parallel to the torsion direction; solid curves represent torsion experiments with foliation perpendicular to the torsion direction.

4. Discussion

In both hydrostatic and dynamic experiments the partial melting of muscovite and quartz produces melt + biotite + sillimanite + K-feldspar as in the previous hydrostatic studies of the quartz–muscovite system (Huang and Wyllie, 1974; Brearley and Rubie, 1990; Haselton et al., 1995; Thompson, 1982). The results also indicate that the melt fraction in

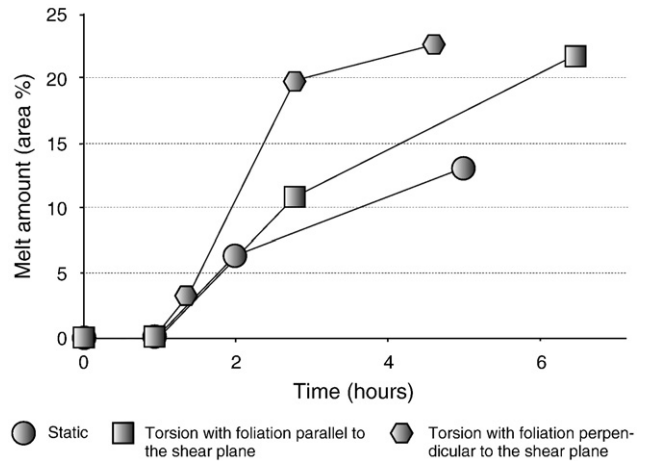


Fig. 6. Amount of melt generation (in area %) in function of time (1 $\gamma \sim 1$ h) in torsion (foliations parallel and perpendicular to the torsion direction) and hydrostatic experiments. Each value is an average of 5 to 6 measurements (statistical error is 2 %).

dynamic experiments is higher than hydrostatic experiments at the same nominal P – T conditions. Misra et al. (2009) also observed that kinetics of partial melt generation is 1.72 times higher in dynamic conditions compared to hydrostatic ones. They suggest four possible explanations for this phenomenon: shear heating, surface energy, strain energy and local pressure drop with subsequent melt movement to explain the difference in reaction kinetics between hydrostatic and dynamic experiments. Here we attempt a first order assessment of the feasibility of each mechanism.

We calculated the magnitude of shear heating (mechanical dissipation) during the torsion experiments from the mechanical data and plotted against shear strain (Fig. 5b). The relation between shear heating (mechanical dissipation) and strain shows that shear heating increases strongly at the onset of the experiments and reaches approximately 10^8 J/m³ at stress peak. Then during weakening the rate of heating decreases and during steady state deformation the heat increases almost linearly. To assess this effect we assume that the energy dissipated mechanically is consumed entirely as latent heat of melting. This assumption implies the process is both isothermal and adiabatic and therefore that there is no effect related to the temperature dependence of diffusion controlled reaction. With these assumptions, our analysis places an upper bound on the amount of melting that may be produced by shear heating. Thus, if the energy released by mechanical dissipation (shear heating) is much less than the difference in latent heat consumed in hydrostatic and dynamic experiments we may exclude shear heating as a possible explanation for increased melting. The energy (E) necessary to explain the difference in reaction progress (E) between the hydrostatic and torsion experiments is:

$$E = \Delta H \times (x_{dyn} - x_{st}) \approx 5 \times 10^8 \frac{J}{m^3}, \quad (1)$$

where ΔH is the enthalpy of the muscovite breakdown reaction (4.5×10^9 J/m³) that was calculated in two different methods, which yielded the same value. In the first method the sum of the enthalpy of mica dehydration and enthalpy of melting were calculated with PerpleX. The second method was to calculate with PerpleX the enthalpy of melt-composed reaction and the same reaction but without melt production. x_{dyn} (0.23) and x_{st} (0.13) are amounts of melt in dynamic and hydrostatic experiments, respectively, after 5 h. The energy dissipated by shear heating (E_{sh}) is

$$E_{sh} = \int (\sigma \times \gamma) dt = 1,8 \times 10^8 \frac{J}{m^3}, \quad (2)$$

where σ (is the shear stress (Fig. 5b) and γ is the shear strain. E_{sh} and E are of comparable magnitudes; therefore theoretically it could be a possible explanation for the increased melt fractions in the dynamic experiments. Taking in the account all the assumptions used in the calculations, higher mechanical dissipation in experiments with sample foliation parallel to the shear plane (in the contrast with melt amount) and high shear strain rate in the experiments in comparison with nature, shear heating should not affect significantly the rate of melting.

The second possible explanation is *surface energy*. During both types of torsion experiments (with different foliation orientations) muscovite is fragmented during deformation processes as a consequence of shear induced grain rotation. Fragmentation leads to the increase of the reactive surface area of quartz and muscovite grains and hence an increase of surface energy. In other words, surface energy is larger in dynamic than in hydrostatic experiments. Initial foliation orientations can also influence and increase surface energy because fragmentation is more common in experiments with foliation perpendicular to the torsion direction, where the elongated grains rotate towards the bulk extension direction and get boudinaged compared to that in the case of foliation parallel to the torsion direction (Fig. 7). Therefore, surface area effect in experiments with foliation parallel to the torsion direction should be less

than in those with foliation perpendicular to the torsion direction. To estimate surface energies we approximate quartz grains as cubes with edge length a and muscovite grains as rectangular parallelepipeds with edges b , c and d . For the hydrostatic 2-hour experiment ($a \sim 10$ μ m, b , c and $d \sim 20$, 5 and 0.5 μ m), the 3-hour torsion experiment with foliation parallel to the shear plane ($a = 7$ μ m, $b = 5$ μ m, $c = 3$ μ m, $d = 0.3$ μ m), and the 3-hour torsion experiment with foliation perpendicular to the shear plane ($a = 5$ μ m, $b = 3$ μ m, $c = 1$ μ m, $d = 0.1$ μ m), the surface areas per unit volume are, respectively, 2×10^5 /m, 6×10^6 /m and 1×10^7 /m, respectively. Experimental studies (e.g., Jurewicz and Watson, 1984; Chen and Navrotsky, 2010) indicate silicate surface energies are in the range of 0.1–5 J/m². Thus, the surface energy effects in our experiments are in the range of 2×10^4 – 5×10^7 J/m³ which are 1 to 4 orders of magnitude smaller than the energy required to explain the increased rate of melting in the shear experiments. Despite this failure, it may be noteworthy that the variation in surface energy between the experiments correlates with reaction rate.

Strain energy theoretically can also be a reason of faster reaction kinetics during deformation than in hydrostatic conditions. To a first approximation strain energy is

$$\delta u^{strain} \approx \frac{15v_0}{4K_s} \Delta\sigma^2 = 2 \text{ J/mol} \quad (3)$$

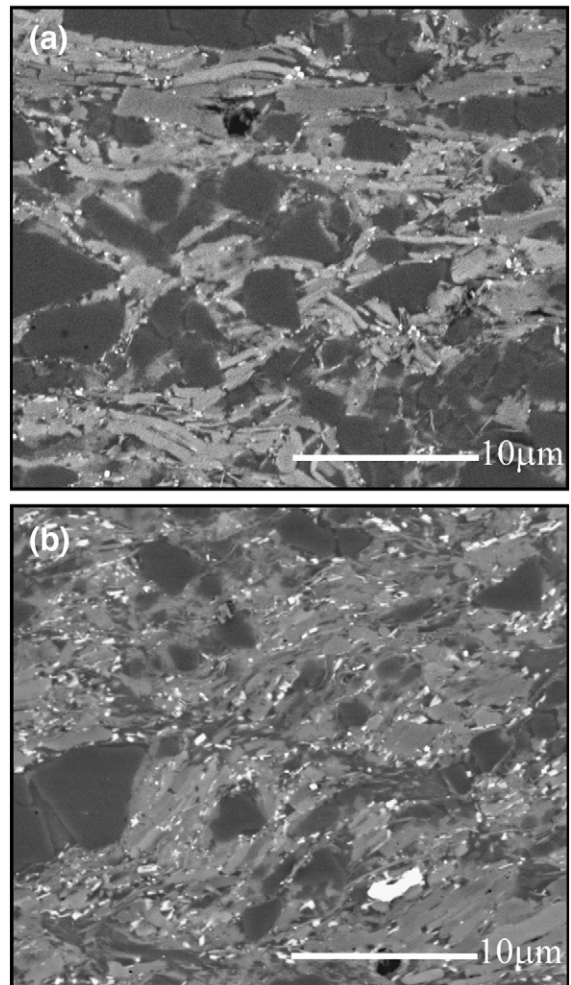


Fig. 7. Microstructures at finite shear strain (γ) 3 in experiments with foliation (a) parallel and (b) perpendicular to the torsion direction. In (a) size of muscovite crystals is smaller (ca 3 μ m in average in the length of the crystals) than in (b) (5 μ m crystal length), indicating crushing process is prominent during torsion of samples with foliation initially perpendicular to the torsion direction. See text for details.

where ν_0 is the volume of unstrained state and K_s is the adiabatic bulk modulus and $\Delta\sigma$ is the shear stress (Connolly, 2009). The bulk properties estimated (Holland and Powell, 1998) for our rock are $\nu_0 = 40 \text{ J/MPa}$, $K_s = 0.3 \times 10^5 \text{ MPa}$; thus, at the steady stress for our experiments (20 MPa), the strain energy is $\sim 5 \times 10^4 \text{ J/m}^3$, which is four orders of magnitude smaller than shear heating and reaction process difference energies. Hence, it should not affect significantly the rate of reaction processes.

Due to shearing local mean stress heterogeneities (melt pressure drop) may develop in the samples. Unequal melt pressure would drive melt movement toward the regions of low mean stress. This process would lead to chemical heterogeneity, such that melt rich domains would be enriched with elements like Si and/or Al; an affect that might lower the melting temperature and enhance melting kinetics. If this model is correct, variations in melt bulk composition along movement paths should be recorded. However, to the extent that it is possible to judge from the Al and Si proportions in the melt phase as measured by EDX-maps of samples of 5 h torsion experiments (P1082), there is no variation in melt composition (Fig. 8). Moreover, the melting of quartz-muscovite rocks tends to be eutectic-like (Thompson and Algor, 1977) and therefore only weakly dependent on bulk composition. For these reasons, we consider that the hypothesis is unlikely to be correct.

Our simple analysis conclusively eliminates all of the explanations for increased melting rate during shear deformation with the possible exception of shear heating. In the case of shear heating, our analysis tests the negative hypothesis of whether energy released by mechanical dissipation is adequate to explain the increased melt production in the adiabatic-isothermal limit. Given that our experimental system is designed to be diathermal, a significant component of the energy dissipated by shear heating may be lost to the environment. For this reason, we regard the shear heating explanation as improbable and therefore propose a new explanation. Specifically we observe that the melting reaction generates a dilational strain of roughly 3% (Connolly et al, 1997); in the elastic limit this strain would generate high pressures that would impede reaction progress (e.g. Mosenfelder et al, 2000). Thus, some component of irreversible dilational deformation is necessary to permit reaction progress. As

pure solids have no intrinsic mechanism of irreversible dilational deformation, irreversible dilation of an aggregate must be accomplished by irreversible microscopic shear processes. These processes may be either viscous or plastic, but for the sake of argument we assume here they are viscous. In the viscous limit, in the dynamic experiments the applied strain rate yields an effective viscosity of $\mu_{eff} = 7 \times 10^{10} \text{ Pa s}$.

The dilational strain rate of a rock that deforms by power-law viscous creep with melt-filled pores at effective pressure P_e (Wilkinson and Ashby, 1975) is

$$\dot{V} = \frac{3A}{2} \left(\frac{3|P_e|}{2n} \right)^n \quad (4)$$

where A and n are material creep parameters. Recasting Wilkinson and Ashby's relation in terms of effective viscosity shows that dilational strain rate is increased by the imposed strain rate:

$$\dot{V} = \frac{3P_e}{4\mu_{eff}} \quad (5)$$

Although the rheological parameters of our sample are unknown, the magnitude of this effect can be assessed by approximating the viscous properties of our sample by those of wet quartzite (Afonso and Ranalli, 2004; Kirby and Kronenberg, 1987). For example, taking the wet quartzite rheology in the absence of macroscopic shear deformation, from Eq. (4) the experimentally observed bulk strain rate would require effective pressures of the order of 1.6 MPa. In contrast, at the experimentally controlled shear strain rate of $3 \times 10^{-4} \text{ s}^{-1}$, Eq. (5) indicates the observed dilational deformation can occur with negligible melt overpressures ($1 \times 10^{-6} \text{ MPa}$). This result suggests that the reduction in effective viscosity induced by macroscopic shear can have a profound effect on reactions that have a non-zero isobaric volume change. The reduction of effective viscosity due to increase of fluid overpressure has been reported as one of the important mechanisms of the piercement structures formation (Mazzini et al., 2009).

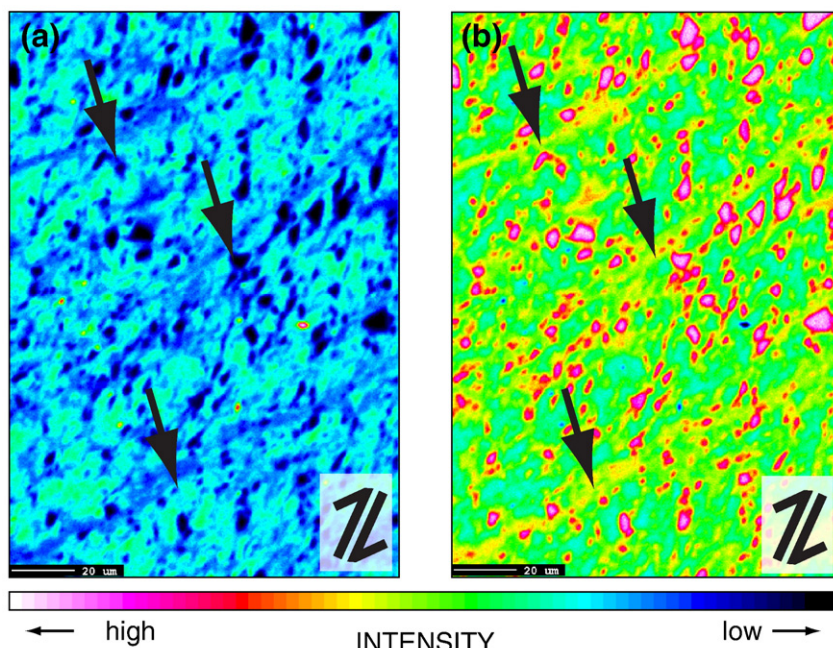


Fig. 8. (a) Al and (b) Si X-ray intensity maps of a torsion experiment (P1082). The arrows indicate melt rich shear bands.

5. Conclusions

We conducted a series of laboratory experiments to demonstrate the role of non-coaxial torsion deformation on partial melting in a quartz–muscovite bearing synthetic rock. The findings of the experimental results are outlined below:

1. At 750 °C and 300 MPa muscovite and quartz react to produce melt, sillimanite, biotite and potassium feldspar.
2. The rate and amount of the melting are dramatically affected by presence of deformation. The deformation greatly enhances the melting process.
3. Pre-existing fabric also influences the rate of partial melting, most probably because of difference in the fragmentation, and hence, in the surface energy.
4. We have considered shear heating, surface energy, strain energy and local pressure drop as explanations for the difference in kinetics between hydrostatic and dynamic experiments that were suggested by Misra et al., 2009. Our calculations show that the magnitude of the energy effect required to explain the increased melting cannot be justified by any of the discussed mechanisms. Only estimated upper bound of shear heating energy has the magnitude of the same order as the energy of additional melting production. However, the shear heating model does not explain the differences in the rate of melting observed in experiments with different foliations. In contrast, surface energy effects increase by an order of magnitude between the hydrostatic experiment and dynamic experiment with foliation parallel to the shear plane and likewise between the dynamic experiments with different foliations. Thus, the effect is consistent with the observed variations in melting kinetics, but the absolute magnitude of the energetic effect is at least one order of magnitude below that required to explain the melting. It is improbable that the strain energy effect is important because it is four orders of magnitude smaller than necessary to explain anomalous melting. The hypothesis that chemical heterogeneity, induced by melt migration, caused the anomalous melting cannot be evaluated quantitatively. However, the facts that pelitic rocks show eutectic like melting which is only weakly sensitive to bulk composition and that we find no evidence for variation in melt composition lead us to reject the hypothesis. We propose a lowering of effective viscosity as an additional explanation of increase in melting rate.

Acknowledgements

We are grateful to Jean-Pierre Burg and Yuri Podladchikov for constructive discussions and the latter in particular for suggesting the role of effective viscosity in enhancing reaction rates. Robert Hoffmann, Karsten Kunze and Claudio Madonna are acknowledged for their technical support in the laboratory, scanning electron microscopy and X-ray element mapping, respectively. This study is a part of a doctoral research project of ETH (No. 0-20480-08) and SNF research grant (200021-116153).

References

Afonso, J.C., Ranalli, G., 2004. Crustal and mantle strengths in continental lithosphere: is the jelly sandwich model obsolete? *Tectonophysics* 394, 221–232.

- Barbey, P., Macaudiere, J., Nzenti, J.P., 1990. High-pressure Dehydration melting of metapelites: evidence from the migmatites of Yaounde (Cameroon). *Journal of Petrology* 31 (Part 2), 401–427.
- Berger, A., Kalt, A., 1999. Structures and melt fractions as indicators of rheology in cordierite-bearing migmatites of the Bayerische Wald (Variscan Belt, Germany). *Journal of Petrology* 40, 1699–1719.
- Brearley, A.J., Rubie, D.C., 1990. Effects of H₂O on the disequilibrium breakdown of muscovite + quartz. *Journal of Petrology* 31, 925–956.
- Chen, S., Navrotsky, A., 2010. Calorimetric study of the surface energy of forsterite. *American Mineralogist* 95, 112–117.
- Clemens, J.D., 1984. Water contents of intermediate to silicic magmas. *Lithos* 11, 213–287.
- Clemens, J.D., Vielzeuf, D., 1987. Constraints on melting and magma production in the crust. *Earth and Planetary Science Letters* 86, 287–306.
- Connolly, J.A.D., 2009. The geodynamic equation of state: what and how. *Geochemistry Geophysics Geosystems* 10 article number 10.
- Connolly, J.A.D., Holness, M.B., Rubie, D.C., Rushmer, T., 1997. Reaction-induced microcracking; an experimental investigation of a mechanism for enhancing anatectic melt extraction. *Geology* 25, 591–594.
- Davidson, C., Schmid, S., Hollister, L., 1994. Role of melt during deformation in the deep crust. *Terra Nova* 6, 133–142.
- De Ronde, A.A., Stünitz, H., 2007. Deformation-enhanced reaction in experimentally deformed plagioclase-olivine aggregates. *Contributions to Mineralogy and Petrology* 153, 699–717.
- Grant, J., 1973. Phase equilibria in high-grade metamorphism and partial melting of pelitic rocks. *American Journal of Science* 273, 289–317.
- Haselton Jr., H.T., Cygan, G.L., Jenkins, D.M., 1995. Experimental study of muscovite stability in pure H₂O and 1 molal KCl–HCl solutions. *Geochimica et Cosmochimica Acta* 59, 429–442.
- Holland, T.J.B., Powell, R., 1998. An internally consistent thermodynamic data set for phases of petrological interest. *Journal of Metamorphic Geology* 16, 309–343.
- Holyoke, C.W., Rushmer, T., 2002. An experimental study of grain scale melt segregation mechanisms in two common crustal rock types. *Journal of Metamorphic Geology* 20, 493–512.
- Huang, W.L., Wyllie, P.J., 1973. Muscovite dehydration and melting in deep crust and subducted oceanic sediments. *Earth Planet Science Letters* 18, 133–136.
- Huang, W.L., Wyllie, P.J., 1974. Melting relations of muscovite with quartz and sanidine in the K₂O–Al₂O₃–SiO₂–H₂O system to 30 kilobars and an outline of paragonite melting relations. *American Journal of Science* 274, 378–395.
- Johannes, W., Holtz, F., 1996. *Petrogenesis and experimental petrology of granitic rocks*. Springer, Berlin, Germany.
- Jurewicz, S.R., Watson, E.B., 1984. Distribution of partial melt in a felsic system: the importance of surface energy. *Contributions to Mineralogy and Petrology* 85, 25–29.
- Keller, L.M., Abart, R., Stünitz, H., De Capitani, C., 2004. Deformation, mass transfer and mineral reactions in an eclogite facies shear zone in polymetamorphic metapelite (Monte Rosa nappe, western Alps). *Journal of Metamorphic Geology* 22, 97–118.
- Kerrick, D.M., 1972. Experimental determination of muscovite + quartz stability with PH₂O < Ptotal. *American Journal of Science* 272, 946–958.
- Kirby, S.H., Kronenberg, A.K., 1987. Rheology of the lithosphere: selected topics. *Reviews of Geophysics* 25, 1219–1244.
- Mazzini, A., Nermoen, A., Krotkiewski, M., Podladchikov, Y., Planke, S., Svensen, H., 2009. Marine and Petroleum Geology 26, 1751–1765.
- Misra, S., Burlini, L., Burg, J.P., 2009. Strain localization and melt segregation in deforming metapelites. *Physics of the Earth and Planetary Interiors* 177, 173–179.
- Mosenfelder, J.L., Connolly, J.A.D., Rubie, D.C., Liu, M., 2000. Strength of (Mg, Fe)₂SiO₄ wadsleyite determined by relaxation of transformation stress. *Physics of the Earth and Planetary Interiors* 120, 63–78.
- Paterson, M.S., Olgaard, D.L., 2000. Rock deformation tests to the large shear strains in torsion. *Journal of Structural Geology* 22, 1341–1358.
- Rubie, D.C., Brearley, A.J., 1987. Metastable melting during the breakdown of muscovite + quartz at 1 kbar. *Bulletin de Mineralogie* 110, 533–549.
- Rushmer, T., 2001. Volume change during partial melting reactions: implications for melt extraction, melt geochemistry and crustal rheology. *Tectonophysics* 342, 389–405.
- Rutter, E., 1997. The influence of deformation on the extraction of crustal melts: a consideration of the role of melt-assisted granular flow. In: Holness, M. (Ed.), *Deformation-Enhanced Melt Segregation and Metamorphic Fluid Transport*, pp. 82–110.
- Thompson, A.B., 1982. Dehydration melting of pelitic rocks and the generation of H₂O-undersaturated granitic liquids. *American Journal of Science* 282, 1567–1595.
- Thompson, A.B., Algor, J.R., 1977. Model systems for anatexis of pelitic rocks. *Contributions to Mineralogy and Petrology* 63, 247–269.
- Vielzeuf, D., Holloway, R., 1988. Experimental determination of fluid-absent melting relations in the pelitic system. Consequences for the crustal differentiation. *Contributions to Mineralogy and Petrology* 98, 257–276.
- Wilkinson, D.S., Ashby, M.F., 1975. Pressure sintering by power law creep. *Acta Metallurgica* 23, 1277–1285.